

Contents

Preface	ix
1 Introduction	1
1.1 Dawning of the Era of Imaging Sciences	1
1.1.1 Image Acquisition	1
1.1.2 Image Processing	5
1.1.3 Image Interpretation and Visual Intelligence	6
1.2 Image Processing by Examples	6
1.2.1 Image Contrast Enhancement	6
1.2.2 Image Denoising	8
1.2.3 Image Deblurring	9
1.2.4 Image Inpainting	9
1.2.5 Image Segmentation	11
1.3 An Overview of Methodologies in Image Processing	12
1.3.1 Morphological Approach	12
1.3.2 Fourier and Spectral Analysis	14
1.3.3 Wavelets and Space-Scale Analysis	15
1.3.4 Stochastic Modeling	16
1.3.5 Variational Methods	17
1.3.6 Partial Differential Equations (PDE's)	19
1.3.7 Different Approaches are Intrinsicly Interconnected	21
1.4 Organization of the Book	23
1.5 How to Read the Book	26
2 Modern Image Analysis Tools	31
2.1 Geometry of Curves and Surfaces	31
2.1.1 Geometry of Curves	31
2.1.2 Geometry of Surfaces in 3-D	36
2.1.3 Hausdorff Measures and Dimensions	44
2.2 Functions with Bounded Variations	45
2.2.1 Total Variation as a Radon Measure	46
2.2.2 Basic Properties of BV functions	49
2.2.3 The Co-Area Formula	52
2.3 Elements of Thermodynamics and Statistical Mechanics	54

2.3.1	Essentials of Thermodynamics	54
2.3.2	Entropy and Potentials	56
2.3.3	Statistical Mechanics of Ensembles	58
2.4	Bayesian Statistical Inference	61
2.4.1	Image Processing or Visual Perception as Inference	61
2.4.2	Bayesian Inference: Bias due to Prior Knowledge	62
2.4.3	Bayesian Method in Image Processing	64
2.5	Linear and Nonlinear Filtering and Diffusion	65
2.5.1	Point Spreading and Markov Transition	65
2.5.2	Linear Filtering and Diffusion	67
2.5.3	Nonlinear Filtering and Diffusion	69
2.6	Wavelets and Multiresolution Analysis	73
2.6.1	Quest for New Image Analysis Tools	73
2.6.2	Early Edge Theory and Marr's Wavelets	75
2.6.3	Windowed Frequency Analysis and Gabor Wavelets	76
2.6.4	Frequency-Window Coupling: Malvar-Wilson Wavelets	77
2.6.5	The Framework of Multiresolution Analysis (MRA)	80
2.6.6	Fast Image Analysis and Synthesis via Filter Banks	86
3	Image Modeling and Representation	89
3.1	Modeling and Representation: What, Why, and How	89
3.2	Deterministic Image Models	91
3.2.1	Images as Distributions (Generalized Functions)	91
3.2.2	L^p Images	94
3.2.3	Sobolev Images $H^n(\Omega)$	96
3.2.4	BV Images	96
3.3	Wavelets and Multiscale Representation	97
3.3.1	Construction of 2-D Wavelets	98
3.3.2	Wavelets Responses to Typical Image Features	102
3.3.3	Besov Images and Sparse Wavelets Representation	105
3.4	Lattice and Random Field Representation	113
3.4.1	Natural Images of Mother Nature	113
3.4.2	Images as Ensembles and Distributions	114
3.4.3	Images as Gibbs Ensembles	115
3.4.4	Images as Markov Random Fields	117
3.4.5	Visual Filters and Filter Banks	120
3.4.6	Entropy Based Learning of Image Patterns	122
3.5	Level-Set Representation	124
3.5.1	Classical Level Sets	125
3.5.2	Cumulative Level Sets	125
3.5.3	Level Sets Synthesis	127
3.5.4	An Example: Level Sets of Piecewise Constant Images	127
3.5.5	High Order Regularity of Level Sets	128
3.5.6	Statistics of Level Sets of Natural Images	129
3.6	Mumford-Shah's Free Boundary Image Model	130
3.6.1	Piecewise Constant 1-D Images: Analysis and Synthesis	130

3.6.2	Piecewise Smooth 1-D Images: First Order Representation	132
3.6.3	Piecewise Smooth 1-D Images: Poisson Representation	133
3.6.4	Piecewise Smooth 2-D Images	134
3.6.5	The Mumford-Shah Model	136
3.6.6	The Role of Special BV Images	138
4	Image Processing: Denoising	143
4.1	Noise: Origins, Physics, and Models	143
4.1.1	Origins and Physics of Noise	143
4.1.2	A Brief Overview of 1-D Stochastic Signals	145
4.1.3	Stochastic Models of Noises	148
4.1.4	Analog White Noises as Random Generalized Functions	149
4.1.5	Random Signals from Stochastic Differential Equations	151
4.1.6	2-D Stochastic Spatial Signals: Random Fields	153
4.2	Linear Denoising: Lowpass Filtering	154
4.2.1	Signal vs. Noise	154
4.2.2	Denoising via Linear Filters and Diffusion	155
4.3	Data-Driven Optimal Filtering: Wiener Filters	157
4.4	Wavelets Shrinkage Denoising	158
4.4.1	Shrinkage: Quasi-Statistical Estimation of Singletons	159
4.4.2	Shrinkage: Variational Estimation of Singletons	161
4.4.3	Denoising via Shrinking Noisy Wavelet Components	164
4.4.4	Variational Denoising of Noisy Besov Images	170
4.5	Variational Denoising Based on BV Image Model	172
4.5.1	Total Variation, Robust Statistics, and Median	172
4.5.2	The Role of Total Variation and BV Image Model	173
4.5.3	Biased Iterated Median Filtering	174
4.5.4	Rudin-Osher-Fatami's TV Denoising Model	175
4.5.5	Computational Approaches to TV Denoising	176
4.5.6	Duality for the TV Denoising Model	181
4.5.7	Solution Structures of the TV Denoising Model	184
4.6	Denoising via Nonlinear Diffusion and Scale-Space Theory	190
4.6.1	Perona and Malik's Nonlinear Diffusion Model	190
4.6.2	Axiomatic Scale-Space Theory	193
4.7	Denoising Salt-and-Pepper Noise	197
4.8	Multichannel TV Denoising	201
4.8.1	Variational TV Denoising of Multichannel Images	201
4.8.2	Three Versions of Total Variations for $TV[\mathbf{u}]$	202
5	Image Processing: Deblurring	205
5.1	Blur: Physical Origins and Mathematical Models	205
5.1.1	Physical Origins	205
5.1.2	Mathematical Models of Blurs	206
5.1.3	Linear vs. Nonlinear Blurs	212
5.2	Illposedness and Regularization	214
5.3	Deblurring with Wiener Filters	215

5.3.1	Intuition on Filter-Based Deblurring	215
5.3.2	Wiener Filtering	216
5.4	Deblurring of BV Images with Known PSF	218
5.4.1	The Variational Model	218
5.4.2	Existence and Uniqueness	221
5.4.3	Computation	222
5.5	Variational Blind Deblurring with Unknown PSF	224
5.5.1	Parametric Blind Deblurring	225
5.5.2	Parametric Field Based Blind Deblurring	228
5.5.3	Non-Parametric Blind Deblurring	231
6	Image Processing: Inpainting	243
6.1	A Brief Review on Classical Interpolation Schemes	244
6.1.1	Polynomial Interpolation	244
6.1.2	Trigonometric Polynomial Interpolation	246
6.1.3	Spline Interpolation	247
6.1.4	Shannon's Sampling Theorem	249
6.1.5	Radial Basis Functions and Thin Plate Splines	251
6.2	Challenges and Guidelines for 2-D Image Inpainting	254
6.2.1	Main Challenges for Image Inpainting	254
6.2.2	General Guidelines for Image Inpainting	256
6.3	Inpainting of Sobolev Images: Green's Formulae	257
6.4	Geometric Modeling of Curves and Images	262
6.4.1	Geometric Curve models	262
6.4.2	2, 3-Point Accumulative Energies, Length, and Curvature	263
6.4.3	Image Models via Functionalizing Curve Models	266
6.4.4	Image Models with Embedded Edge Models	268
6.5	Inpainting BV Images (via the TV Radon measure)	269
6.5.1	Formulation of the TV Inpainting Model	269
6.5.2	Justification of TV Inpainting by Visual Perception	270
6.5.3	Computation of TV Inpainting	272
6.5.4	Digital Zooming Based on TV Inpainting	273
6.5.5	Edge Based Image Coding via Inpainting	274
6.5.6	More Examples and Applications of TV Inpainting	275
6.6	Error Analysis for Image Inpainting	277
6.7	Inpainting Piecewise Smooth Images via Mumford-Shah	280
6.8	Image Inpainting via Euler's Elastica and Curvatures	283
6.8.1	Inpainting Based on the Elastica Image Model	283
6.8.2	Inpainting via Mumford-Shah-Euler Image Model	285
6.9	Inpainting of Meyer's Texture	287
6.10	Image Inpainting with Missing Wavelet Coefficients	290
6.11	PDE Inpainting: Transport, Diffusion, and Navier-Stokes	292
6.11.1	Second Order Interpolation Models	293
6.11.2	A 3rd Order PDE Inpainting Model and Navier-Stokes	298
6.11.3	TV Inpainting Revisited: Anisotropic Diffusion	299
6.11.4	CDD Inpainting: Curvature Driven Diffusion	300

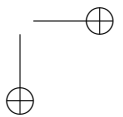
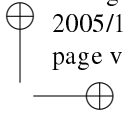
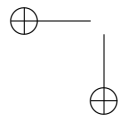
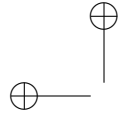
Contents v

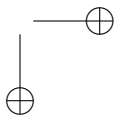
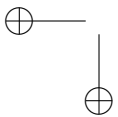
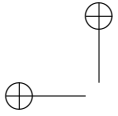
- 6.11.5 A Quasi-Axiomatic Approach to 3rd Order Inpainting . . . 301
- 6.12 Inpainting of Gibbs/Markov Random Fields 305

- 7 Image Processing: Segmentation 309
 - 7.1 Synthetic Images: Monoids of Occlusive Preimages 309
 - 7.1.1 Introduction and Motivation 309
 - 7.1.2 Monoids of Occlusive Preimages 310
 - 7.1.3 Mimimal and Prime (or Atomic) Generators 315
 - 7.2 Edges and Active Contours 318
 - 7.2.1 Pixelwise Characterization of Edges: David Marr's Edges 318
 - 7.2.2 Edge-Regulated Data Models for Image Gray Values . . . 320
 - 7.2.3 Geometry-Regulated Prior Models for Edges 322
 - 7.2.4 Active Contours: Combining Both Prior and Data Models 326
 - 7.2.5 Curve Evolutions via Gradient Descent 327
 - 7.2.6 Γ -Convergence Approximation of Active Contours 329
 - 7.2.7 Region Based Active Contours Driven by Gradients 331
 - 7.2.8 Region Based A.C. Driven by Stochastic Features 333
 - 7.3 Geman-Geman's Intensity-Edge Mixture Model 338
 - 7.3.1 Topological Pixel Domains, Graphs, and Cliques 339
 - 7.3.2 Edges as Hidden Markov Random Fields 340
 - 7.3.3 Intensities as Edge-Regulated Markov Random Fields . . . 342
 - 7.3.4 Gibbs's Fields for Joint Bayesian Estimation of u and Γ . 343
 - 7.4 Mumford-Shah's Free-Boundary Segmentation Model 344
 - 7.4.1 The Mumford-Shah Segmentation Model 344
 - 7.4.2 Asymptotic M.-S. Model I: Sobolev Smoothing 346
 - 7.4.3 Asymptotic M.-S. Model II: Piecewise Constant 348
 - 7.4.4 Asymptotic M.-S. Model III: Geodesic Active Contours . 352
 - 7.4.5 Non-Uniqueness of M.-S. Segmentation: A 1-D Example 355
 - 7.4.6 Existence of M.-S. Segmentation 356
 - 7.4.7 How to Segment Sierpinski Islands 360
 - 7.4.8 Hidden Symmetries of M.-S. Segmentation 363
 - 7.4.9 Computational Method I: Γ -Convergence Approximation 365
 - 7.4.10 Computational Method II: Level-Set Method 367
 - 7.5 Multi-Channel Logical Segmentation 370

- Bibliography 375

- Index 396





List of Figures

1.1 An ideal image: noiseless, complete, and in good contrast. 7

1.2 A low-contrast version of the ideal image. 7

1.3 Degradation by additive Gaussian noise (Chapter 4). 8

1.4 Salt-and-pepper noise with 10% spatial density (Chapter 4). 9

1.5 Degradation by out-of-focus blur: The digital camera focuses on a finger-
tip about 1 inch away while the target scene is about 1 foot away (Chapter
5). 10

1.6 Degradation by motion blur due to horizontal hand jittering during a
single exposure (Chapter 5) 10

1.7 150 8-by-8 packets are randomly lost during transmission (Chapter 6).
The goal of error concealment (or more generally, inpainting) is to develop
models and algorithms that can automatically fill in the blanks [24, 67, 166]. 11

1.8 Such cartoonish segmentation seems trivial to human vision, but still
remains the most fundamental and challenging problem in image pro-
cessing and low-level computer vision (Chapter 7). (The background
segment Ω_0 is not shown explicitly here.) 11

1.9 A binary set A and a structure element S (for dialation and erosion). . . . 13

1.10 Dialation $D_S(A)$ (left) and erosion $E_S(A)$ (right): dilation closes up
small holes or gaps, while erosion opens them up. 14

1.11 A digital image and its discrete Fourier transform. The example reveals
a couple of salient features of Fourier image analysis: (1) most high-
amplitude coefficients concentrate on the low-frequency band; (2) dom-
inant directional information in the original image is easily recognizable
in the Fourier domain; and (3) the coefficients however decay slowly for
Heaviside-type directional edges (i.e., a jump line with distinct constant
values along its two shoulders). 15

1.12 An example of a (mother) wavelet by Daubechies' design [96]. Local-
ization and oscillation are characteristic to all wavelets. 16

1.13 A noisy 1-D signal and its optimal restoration according to (1.7). 19

1.14 A trefoil evolves under mean-curvature motion (1.11) or (1.12). 21

1.15 Different approaches are intrinsically connected: An example. 22

1.16 Organization of the book. 25

2.1 A planar curve: tangent \mathbf{t} , normal \mathbf{n} , and curvature κ 32

2.2	Second order local geometry: surface normal N and two perpendicular principle curvature circles.	38
2.3	A surface patch $z = h(u, v) = \cos(u) \cos(v)$ (top), its mean curvature field H (lower left) and Gauss curvature field K (lower right).	40
2.4	A set E (left) and a covering \mathcal{A} (right). Covering elements like the huge box with dashed borders (right) fail to faithfully capture small scale details. The definition of Hausdorff measures forces covering scales to tend to zero.	44
2.5	The Hausdorff dimension $\dim_H(E)$ of a set E is the critical d , above which E appears too “thin,” while below too “fat.”	45
2.6	Three 1-D images with $\text{TV}[f] = \text{TV}[g] = \text{TV}[h] = 2$	47
2.7	An example of L^1 -lower semicontinuity. The sequence (u_n) of 1-D images on $[0, 1]$ converge to $u = 0$ in L^1 since $\ u_{n+1} - u\ _{L^1} \leq 2^{-n}$. Notice that $\text{TV}(u) = 0$ while $\text{TV}(u_n) \equiv 2$, which is consistent with the property of lower semicontinuity: $\text{TV}(u) \leq \liminf_n \text{TV}(u_n)$. In particular, strict inequality is indeed realizable.	49
2.8	Geometric meaning of total variation: the co-area formula. For smooth images, $\text{TV}(u)$ is to sum up the lengths of all the level curves, weighted by the Lebesgue element $d\lambda$. Plotted here is a discrete approximation: $\text{TV}(u) \simeq \sum_n \text{length}(u \equiv \lambda_n) \Delta\lambda$	54
2.9	Gibbs’ canonical ensemble: higher temperature T corresponds to smaller β and more uniform distribution; on the other hand, when $T \simeq 0$, the system exclusively remains at the ground state (leading to superfluids or superconductance in physics).	59
2.10	Gibbs’ entropies for two imaginary 4-state systems (with κ set to 1). Entropy generally measures the degrees of freedom of a system. A lower entropy therefore means that the target system is more restrained. (This observation led Shannon [272] to define negative entropies as information metrics, since less randomness implies more information.)	60
2.11	An example of linear anisotropic diffusion by (2.38) with diagonal diffusivity matrix $D = \text{diag}(D_x, D_y)$ and $D_y : D_x = 10 : 1$. The image thus diffuses much faster along the vertical y -direction.	68
2.12	The median of a 5-component segment from an imaginary 1-D signal (x_n)	70
2.13	An example of using the median filter (with 7×7 centered square window) to denoise an image with severe salt-and-pepper noise. Notice the outstanding feature of median filtering: the edges in the restored image are not blurry.	71
2.14	Two examples of Marr’s wavelets (“Mexican hats”) as in (2.50).	75
2.15	A generic approach to designing the window template $w(x)$ via symmetrically constructing the profile of its square $w^2(x)$	79
2.16	Multiresolution analysis as (Hilbert) space decompositions: the finer resolution space V_2 is decomposed to the detail (or wavelets) space W_1 and coarser resolution space V_1 . The same process applies to V_1 , and all other V_j ’s [290].	84

List of Figures ix

2.17 A pair of compactly supported scaling function $\phi(x)$ and mother wavelet $\psi(x)$ by Daubechies' design [96]. 86

2.18 Fast wavelets transform via filter banks: the 2-channel analysis (or decomposition) and synthesis (or reconstruction) banks. 88

3.1 Images as distributions or generalized functions. Test functions then model various biological or digital sensors, such as retinal photoreceptors of human vision or coupled charge devices in CCD cameras. 92

3.2 Three Haar mother wavelets in 2-D via tensor products. 101

3.3 Besov norms in $B_q^\alpha(L^p)$'s measure the strength of signals in the space-scale plane: L^p for intra-scale variations, L^q for inter- or cross-scale variations (in terms of $d\lambda = dh/h$), while $h^{-\alpha}$ for comparison with Hölder continuity. 107

3.4 Ingredients of Markov random fields by examples: a neighborhood N_α (left), two doubleton cliques $C \in \mathcal{C}$ (middle), and locality of conditional inference $p(u_\alpha | u_{\Omega \setminus \alpha}) = p(u_\alpha | u_{N_\alpha})$ (right). 118

3.5 An Example of branches $L_{\lambda, \Delta\lambda}$'s with $\Delta\lambda = h$ and $\lambda = nh$. The branch $L_{3h, h}$ contains two leaflets. 130

3.6 The (x_n, b_n, g_n) -representation of a (compactly supported) piecewise smooth signal u . On smooth regions where the signal u varies slowly, g_n is often small and only a few bits suffice to code them. 133

3.7 Poisson representation of a piecewise smooth signal u . Shown here is only a single representative interval. The signal u is represented by the two boundary values u_n^+ and u_{n+1}^- , and its second order derivative $f = u''$ (corresponding to the source distribution in electromagnetism). Reconstructing u on the interval then amounts to solving the Poisson equation (3.62). The advantage of such representation is that f is often small (just like wavelet coefficients) for smooth signals, and demands much less amount of bits compared with u 134

4.1 A sample 2-D Brownian path $W(t)$ with $0 < t < 4$, and the reference circle with radius $2 = \sqrt{4}$, the standard deviation of $W(4)$ 150

4.2 A sample random signal generated by the SDE: $dX = 2Xdt + XdW$ with $X(0) = 1$. The smooth dashed curve denotes the mean curve $x(t) = EX(t) = e^{2t}$. The random signal is clearly not stationary since both the means and variances of $X(t)$ evolve. 153

4.3 Hard thresholding $T_\lambda(t)$ and soft shrinkage $S_\lambda(t)$ 159

4.4 The shrinkage operator $\hat{a}_* = S_\sigma(a_0)$ achieves minimum shrinkage (Theorem 4.4) among all the estimators \hat{a} that satisfy the uniform shrinkage condition (4.25). 161

4.5 Two singleton error functions $e_1(t|a_0)$ with $\lambda = \mu = 1$ and $a_0 = 1, 2$. Notice that the optimal estimators (i.e., the valleys) $\hat{a} = 0, 1$ are precisely the shrinkages $S_\sigma(a_0)$, with $\sigma = \mu/\lambda = 1$ 163

4.6	An example of shrinkage based image denoising, with Gaussian white noise level $\sigma = 0.1$, and 4 levels of wavelet decompositions based on one of Daubechies' orthonormal wavelets [96]. The three bottom panels demonstrate the effect of the threshold parameter λ for the shrinkage operator S_λ : a too large λ causes over shrinkage and over smoothing, while a too small one leads to the opposite.	169
4.7	Same example as in Figure 4.6 with increased Gaussian noise level $\sigma = 0.2$.	170
4.8	Denoising effects of moving means v.s. moving medians. Both employ the same symmetric (moving) window of four neighbors on either side. As expected, the median filter preserves sharp edges better than the mean filter. (The dashed curve denotes the ideal clean signal.)	173
4.9	An example of Rudin-Osher-Fatemi's TV denoising.	178
4.10	A target pixel O and its neighbors	180
4.11	An example of applying Perona-Malik's anisotropic diffusion to a noisy image. The nonlinear diffusivity coefficient $D(\nabla u)$ for this example is the one in (4.93) and (4.94). Notice the remarkable feature of edge preservation, as contrast to linear heat diffusions that invariably blur sharp edges while removing noises.	192
4.12	Two examples of salt-and-pepper noises and the denoising performance of median filtering. As consistent with theoretical analysis, median filtering works very efficiently for low spatial densities but poorly for high ones.	200
4.13	An example of applying the TV inpainting technique (4.103) (also see Chan and Shen [67] or Chapter 6) to the denoising of high density salt-and-pepper noises.	201
5.1	An example of motion blur (due to camera jittering)	207
5.2	Motion blur of the image of a point source	208
5.3	An example of out-of-focus blur	210
5.4	Geometric optics of out-of-focus imaging	211
5.5	An example of Wiener filtering for both denoising and deblurring.	217
5.6	Deblurring an out-of-focus image (with known PSF).	223
5.7	Deblurring an image blurred by horizontal hand jittering.	224
5.8	Another example of restoring an image blurred by motion.	224
5.9	A computational example for the double-BV blind deblurring model (by Chan and Wong [77]). Left: the blurry image; Right: the deblurred image.	242
6.1	The goal of inpainting is to reconstruct the ideal image u on the entire domain based on the incomplete and often degraded data u^0 available outside the missing (or inpainting) domain D	244
6.2	The effect of local and global pattern recognition on image inpainting: the black color seems to be a reasonable inpainting solution in the left panel, while for the right chessboard pattern, the white color becomes more plausible (chan and Shen [67]).	255
6.3	The effect of aspect ratios on image inpainting [67].	256

6.4	Harmonic inpainting of a smooth image ($u = r = \sqrt{x^2 + y^2}$) and an ideal step edge.	261
6.5	Can the TV inpainting model explain Kanizsa's Entangled Man?	271
6.6	The model for Kanizsa's Entangled Man.	272
6.7	Inpainting a noisy edge.	276
6.8	Inpainting occluded bars.	276
6.9	Inpainting a noisy face.	276
6.10	Inpainting for text removal.	276
6.11	Digital harmonic zoom-in and TV zoom-in (Chan and Shen [67]).	277
6.12	Edge decoding by TV inpainting (Chan and Shen [67]; also see the recent pattern-theoretic approach by Guo, Zhu, and Wu [148]).	278
6.13	The aspect ratios of inpainting domains influence the performance of inpainting schemes (Chan and Kang [59]).	279
6.14	Inpainting based on the Γ -convergence approximation (6.42) and its associated elliptic system (6.47).	282
6.15	Text erasing by inpainting based on the Mumford-Shah image model.	282
6.16	Two examples of elastica inpainting, as compared with TV inpainting. In the case of large aspect ratios [68], the TV inpainting model fails to comply to the Connectivity Principle.	285
6.17	Inpainting based on the Mumford-Shah-Euler image model can satisfactorily restore a smooth edge as expected.	287
6.18	An example of inpainting a noisy and incomplete BV image with missing wavelet components using the model (6.64) (Chan, Shen, and Zhou [74]).	293
6.19	Another example of inpainting a noisy and incomplete BV image with missing wavelet components using the model (6.64) (Chan, Shen, and Zhou [74]).	293
6.20	TV fails to realize the Connectivity Principle in inpaintings with large scales (or aspect ratios).	300
6.21	An example of CDD inpainting for scratch removal.	301
7.1	Role of occlusion in visual perception. Left panel: a gray vase against a bright background or two opposite human faces against a gray background? This is a typical illusion problem caused by the lack of occlusion cues; Right panel (a trefoil): the role of occlusion in knot theory [253].	310
7.2	An example of two preimages a_γ and b_δ and their occlusion $a_\gamma \dashv b_\delta$. Complex images patterns in the real world often originate from simple objects via occlusion.	312
7.3	Left: a diskette preimage; Right: a planar preimage.	316
7.4	On an edge pixel x (with $\gamma(x) = 1$), $p = \nabla u (x)$ is more likely to be large according to (7.17).	322
7.5	An example of geodesic active contouring: the given image and three different stages of the contour evolution by (7.32).	329
7.6	An example of Chan and Vese's active contour model (7.52) without gradients (i.e., region based and driven by mean fields): three different evolution stages for a sectional brain image (from Chan and Vese [75]).	338

7.7 An example of texture segmentation by combining Chan and Vese’s active contour model (7.52) and Gabor filters (7.53) (shown at increasing times; see Sandberg, Chan, and Vese [65, 260]). 339

7.8 A pixel lattice $\Omega = \{a, b, \dots\}$ and an edge lattice $E = \{\alpha, \beta, \dots\}$ 341

7.9 Six binary edgel configurations on a maximal edge clique, and their empirical potentials $V_C^E(\Gamma)$ ’s assigned by Geman and Geman [130] (where A is a constant). 342

7.10 The total curvatures (in the interior of the pixel squares) of closed tours around the six edge configurations qualitatively match Geman and Geman’s empirical choice of potentials in Figure 7.9. 343

7.11 Visualization of the Example: the set S consisting of the circles at all scale levels has the weird property: $\mathcal{H}^1(S) < \infty$ but $\mathcal{H}^1(\bar{S}) = \infty$, since $\bar{S} = \Omega$ 358

7.12 Left Panel: the complement G of the classical Sierpinski gasket (Mandelbrot [206]) consists of all the shaded open triangles (excluding their sides). Right Panel: Sierpinski Islands $G(\rho)$ is the open set obtained from G by contracting each triangle of G with some suitable rate controlled by some $\rho \in (0, 3/2)$ (see the text). And the target image u_ρ discussed in this section is the indicator function of $G(\rho)$ 361

7.13 An example of Γ -convergence based approximation to the Mumford-Shah segmentation model (7.97): the optimal image estimation $u = u_\epsilon(x)$ and its associated edge “canyon” function $z = z_\epsilon(x)$. Computation has been based on the alternating minimization scheme (7.98). 367

7.14 An example of Mumford-Shah segmentation using the level-set algorithm by Chan and Vese [75, 76]. 370

7.15 A synthetic example of an object in two different channels. Notice that the lower left corner of A_1 and the upper corner of A_2 are missing. 370

7.16 Different logical combinations for the sample image: the union, the intersection, and the differentiation. 371

7.17 Region based logical model on a medical image. In the first channel A_1 , the noisy image has a “brain tumor”, while channel A_2 does not. The goal is to spot the tumor that is in channel A_1 , but not in A_2 , i.e., the differentiation $A_1 \cap \neg A_2$. In the right column, we observe that the tumor has been successfully captured. 373